International Journal of Nanomedicine

Dovepress
open access to scientific and medical research

Open Access Full Text Article

ORIGINAL RESEARCH

Multifunctional Nano-Realgar Hydrogel for Enhanced Glioblastoma Synergistic Chemotherapy and Radiotherapy: A New Paradigm of an Old Drug

Yihan Wang[1,2], Yizhen Wei[1,2], Yichun Wu[1,2], Yue Zong[1,2], Yingying Song[2], Shengyan Pu[2], Wenwen Wu[2], Yun Zhou[1], Jun Xie[2], Haitao Yin[1]

[1]Department of Radiotherapy Central Hospital, Affiliated Xuzhou Clinical College of Xuzhou Medical University, Xuzhou, 221009, People's Republic of China; [2]Key Laboratory for Biotechnology on Medicinal Plants of Jiangsu Province, School of Life Science, Jiangsu Normal University, Xuzhou, 221116, People's Republic of China

Correspondence: Haitao Yin; Jun Xie, Email yinhaitao@njmu.edu.cn; xiejun@jsnu.edu.cn

Purpose: Realgar, as a kind of traditional mineral Chinese medicine, can inhibit multiple solid tumor growth and serve as an adjuvant drug in cancer therapy. However, the extremely low solubility and poor body absorptive capacity limit its application in clinical medicine. To overcome this therapeutic hurdle, realgar can here be fabricated into a nano-realgar hydrogel with enhanced chemotherapy and radiotherapy (RT) ability. Our objective is to evaluate the superior biocompatibility and anti-tumor activity of nano-realgar hydrogel.

Methods: We have successfully synthesized nano-realgar quantum dots (QDs) coupling with 6-AN molecules (NRA QDs) and further encapsulated with a pH-sensitive dextran hydrogel carrier with hyaluronic acid coating (DEX-HA gel) to promote bioavailability, eventually forming a multifunctional nano-realgar hydrogel (NRA@DH Gel). To better investigate the tumor therapy efficiency of the NRA@DH Gel, we have established the mice in situ bearing GL261 brain glioblastoma as animal models assigned to receive intratumor injection of NRA@DH Gel.

Results: The designed NRA@DH Gel as an antitumor drug can not only exert the prominent chemotherapy effect but also as a "sustainable reactive oxygen species (ROS) generator" can inhibit in the pentose phosphate pathway (PPP) metabolism and reduce the production of nicotinamide adenine dinucleotide phosphate (NADPH), thereby inhibiting the conversion of glutathione disulfide (GSSG) to glutathione (GSH), reducing GSH concentrations in tumor cells, triggering the accumulation of ROS, and finally enhancing the effectiveness of RT.

Conclusion: Through the synergistic effect of chemotherapy and RT, NRA@DH Gel effectively inhibited the proliferation and migration of tumor cells, suppressed tumor growth, improved motor coordination, and prolonged survival in tumor-bearing mice. Our work aims to improve the NRA@DH Gel-mediated synergistic chemotherapy and RT will endow a "promising future" for the old drug in clinically comprehensive applications.

Keywords: NRA@DH Gel, glioma, inhibition of the PPP, ROS, radiosensitization, synergistic therapy

Introduction

Brain gliomas are the most common and fatal primary tumors among central nervous system malignancies. The standard of care is surgical resection followed by radiotherapy (RT) and chemotherapy, but the prognosis is extremely poor[1,2] Clinical chemotherapeutic drugs are typically associated with common limiting features, including a single variety, poor targeting, high doses, strong toxicity, and significant side effects that are not easily tolerated. Conventional fractionated radiotherapy (RT) is often applied in clinical practice. However, it is prone to radiation-induced brain injuries, such as vasodilatation, blood–brain barrier impairment, leucoencephalopathy, and radiation necrosis.[3–5] Additionally, the hypoxic environment of tumors and the removal of reactive oxygen species (ROS) produced by intracellular antioxidants can cause radiochemotherapy resistance and reduce the corresponding efficacy.[6–8] The tumor microenvironment can be characterised by low pH, hypoxia, high

Received: 1 November 2022
Accepted: 2 February 2023
Published: 14 February 2023

concentrations of glutathione (GSH), and specific expression of enzymes. As a vital component of the antioxidant system, GSH scavenges ROS in the body. However, stabilisation of the redox state is destroyed by the consumption of GSH, resulting in ROS accumulation. Under the action of nicotinamide adenine dinucleotide phosphate (NADPH), glutathione disulfide (GSSG) can be converted into GSH, which is a source of intracellular GSH. Therefore, NADPH is essential for the reduction process. A competitive inhibitor of 6-Phosphogluconate Dehydrogenase (G6PDH) is 6-Aminonicotinamide (6-AN), which is a key enzyme in the pentose phosphate pathway. NADPH production is reduced by the inhibition of the pentose phosphate pathway (PPP), thereby blocking the conversion of GSSG to GSH.[9–12] Reducing intracellular GSH level is beneficial for many cancer therapeutic regimens.

In the past few years, with the rapid development of nanotechnology, the use of nanotechnology has been considered as a promising strategy to improve the therapeutic effect of cancer RT. Nanomaterials have numerous advantages, such as good biocompatibility, high drug-loading capacity, and an enhanced permeability and retention effect (EPR) effect in tumor tissues. The application of nano-RT sensitisers can promote the sensitivity of tumors to ionising radiation and decrease the damage to normal tissues while enhancing the curative effect of RT. Currently, numerous nanoparticles (NPs) have been developed for effective RT, which can inhibit tumor growth by enhancing the deposition of radiation energy in cells, and then target the ROS with their killing effects, leading to excellent radiotherapy sensitivity.[13–16]

In glioma therapy, conventional chemotherapy methods can easily cause hematological toxicity and even induce epilepsy. The structural redesign of traditional chemotherapeutic drugs and improvement of dosage can reduce toxicity and side effects, thereby enhancing the efficacy of the drugs. Arsenic is a traditional Chinese mineral medicine, which has been used as an anti-inflammatory and antibacterial medicine in ancient times.[17–20] Modern medicine has also demonstrated arsenic as an effective chemotherapeutic drug and that it can be used in various tumor treatments. For example, arsenic oxide therapy combined with all-trans retinoic acid has already become the first-line treatment for acute promyelocytic leukaemia (APL). However, its toxicity and side effects limit its widespread clinical application.[21–24] Realgar, an important ore of arsenic, has higher biosafety than that of arsenic oxide, and it can effectively induce tumor cell apoptosis, inhibit angiogenesis, restrain tumor liver and lung metastasis, and prolong patient survival time.[25,26] Conversely, the low solubility and poor bioavailability of traditional realgar is not conducive to its clinical application. To improve its curative effect on tumors, realgar can be fabricated at the nanometre scale or encapsulated with a hydrophilic polymer to promote bioavailability.[27–30] When the realgar particle size is decreased to the ultra-fine nanometre scale, it displays excellent fluorescence properties, resembling quantum dots (QDs), and also superior biocompatibility and anti-tumor activity.[31–35]

Drug carriers with good biocompatibility play a crucial role in successfully maximizing the delivery of drugs to tumor regions. In recent years, biomacromolecule hydrogels have been rapidly developed into a new type of drug delivery system, providing biological safety, as well as sustained and controlled release.[36–39] An intelligent biomacromolecule hydrogel is a hydrophilic, three-dimensional, network-structured gel. After specific and functional modifications, the intelligent biomacromolecule hydrogel becomes an environmentally responsive gel that can be used for drug loading. The corresponding physical structure and chemical properties can be changed by sensing variations in the external environment or stimuli to achieve sustained drug release.[40–43]

In the present study, we designed high-performance nano-realgar QDs coupled with 6-AN molecules (NRA QDs) with excellent fluorescent properties and potential medicinal efficacy. NRA QDs were then enveloped with pH-sensitive dextran hydrogel with hyaluronic acid coating (DEX-HA gel) to form a multifunctional nano-realgar hydrogel (NRA@DH Gel). We believe the NRA@DH Gel has utility as an anti-tumor drug by inducing a potent chemotherapy effect and as a "sustainable ROS generator" for enhancing the efficacy of RT. The use of NRA@DH Gels as a synergistic therapy for tumors presents a "promising future" for this old drug in a wide range of clinical applications.

Materials and Methods

Materials

Pure realgar powders (RP; Medical-Grade, 99%) were obtained from Xi′an Tianzheng Pharmaceutical Adjuvant Co., Ltd (China). Methanol, 1-ethyl-3-(dimethylaminopropyl) carbodiimide hydrochloride (EDC), N-hydroxysuccinimide (NHS),

and 2-(N-morpholino) ethanesulfonic acid (MES) were obtained from Aladdin Chemical Reagent Co., Ltd (China). Hyaluronic acid (HA), and paraformaldehyde were purchased from Sinopharm Chemical Reagent Co., Ltd (China). Dextran (DEX), NaIO4, 6-AN were purchased from Shanghai Macklin Biochemical Co., Ltd (China). PEG_{2000} (NH_2-PEG2000-COOH; NPC) and PEG_{2000} (NH_2-PEG2000- NH_2; NPN) were purchased from Shanghai Ponsure Biotechnology Co., Ltd (China). Deionized water was supplied by a Q-POD water purification machine (Millipore, MA, USA). PEG200 was purchased from Beijing Solarbio Science & Technology CO., Ltd. (China).

The rabbit anti-CD31, Ki-67, and HIF-1α primary antibodies, and horseradish peroxidase (HRP)-labeled goat antirabbit secondary antibodies were purchased from Servicebio Technology Co., Ltd. (China). The CCK-8 assay kits, JC-1 kit, Masson trichrome kit, SDS-PAGE gel preparation kit, and cell apoptosis detection kit (containing Annexin V-FITC/PI) were purchased from KeyGEN Biotechnology Co., Ltd. (China). The ROS assay kit and the GSSG assay kit were purchased from Beijing Solarbio Science & Technology CO., Ltd. (China). The GSH assay kit was purchased from Beijing Boxbio Science & Technology CO., Ltd. (China). The mouse γH2AX ELISA kit was purchased from Shanghai Xuanke Biotechnology CO., Ltd. (China).

Preparation of NRA@ DH Gel

For the NRA QDs synthesis, we first took 500 mg RP mixed with 50 mg NPC in the presence of PEG200 (high boiling solvent) at 250 °C for 8 h via coordination chemical reaction to form arsenic atoms (present in NR QDs) with carboxy terminus (NR@COOH QDs) by nucleation and growth process. Next, 60 mg EDC and 80 mg NHS were added in the above solution at 37 °C and shaken for 30 min at 37 °C to activate the carboxyl terminal of NR@COOH QDs dispersed in 10 mL of MES buffer (0.02 $mol \cdot L^{-1}$) at pH 5.4. After ultrafiltration centrifugation, the active NR@COOH QDs intermediates were further coupled with the 6-AN molecules in boric acid buffer (0.02 $mol \cdot L^{-1}$) at pH 8.4, eventually obtaining the NRA QDs.

For pH-sensitive DEX Gel drug carrier synthesis, we took 0.5 g of DEX powder dissolving and swelling in deionized water, and then added 20 mg $NaIO_4$ stirring 50 °C for 6 h to form the oxidized dextran (ODEX) Gel with aldehyde terminus. After adding 30 mg functionalized NPN powder on the magnetic stir plate for 6~8 hours at 50 °C, the pH-sensitive amide bonds were then introduced by the reaction of Schiff base reaction on the aldehyde groups in ODEX Gel, forming the DEX Gel with amino terminals (DEX-NH_2 Gel). Next, 0.2 g HA powder was dissolved in deionized water, and this was followed by adding EDC/NHS at room temperature for 30 min to activate the carboxyl group. The DEX-NH_2 Gel was then coupled with activated HA molecules, mixed and stirred for 4 h, forming the DEX-HA gel with active targeting ability. Finally, the above-mentioned NRA QDs were wrapped in DEX-HA gel by physical embedding using magnetically stirred for 4 h, eventually obtaining NRA@DH Gel.

Characterization

The physical and chemical properties of NRA@DH Gel were characterized by the morphology, optical property, rheologic behavior, as well as chemical and elemental analyses. Specifically, the morphology and elemental distribution of NRA@DH Gel were, respectively, characterized by transmission electron microscopy (TEM; JEOL, Japan) and scanning electron microscopy (SEM; Hitachi S-4800, Japan). The composition and structure of NRA@DH Gel were measured by Fourier transform infrared spectroscopy (FT-IR; Bruker, Germany). The absorption spectrum of NRA@DH Gel was performed using a UV−vis spectrophotometer (Shimadzu UV-2501PC, Japan). The fluorescence emission spectrum of NRA@DH Gel was measured by a fluorescence spectrophotometer (Shimadzu F-7000, Japan) and corresponding fluorescence imaging was carried out on a fluorescence imaging system (Caliper Life Sciences, USA) with excitation of 610 nm filter and emission of 840 nm filter. The rheological properties of NRA@DH Gel were performed on a rotated rheometer (Anton Paar, Germany) with a PP25 coaxial cylinder geometry. The chemical structure of NRA@DH Gel was recorded using an in Via Raman microscope (Renishaw, UK).

In vitro Release of NRA QDs

The in vitro release characteristic of NRA QDs embedding in pH-responsive NRA@DH Gel was investigated by a dialysis method. Specifically, the NRA@DH Gel was put into a dialysis bag (MD:7000KD) at 37°C and dipped in

50 mL PBS with gentle shaking at pH 7.4, 6.5, and 5.5 over a period of 72 h. The optical density (OD) values of NRA@DH Gel inside the dialysis bag were then measured using a UV–vis spectrophotometer (Shimadzu, UV-2501PC, Japan) at 450 nm wavelength (characteristic peak of NRA@DH Gel) at different times. The in vitro release rate (RR) of NRA QDs was calculated as follows: $RR = (A_0 - A_t)/A_0$ (A_0 represents the initial absorbance of NRA@DH Gel solution at 450 nm, and at represents the real-time absorbance of NRA@DH Gel under the different conditions). Drug release curves were ultimately obtained by plotting cumulative drug release against time.

Cell Culture

The Mice brain glioma cancerous (GL261) cells were purchased from Cell Bank, Chinese Academy of Sciences (Shanghai, China), and then cultured in DMEM media supplemented with 10% fetal bovine serum (FBS) and 1% penicillin–streptomycin mixed antibiotics containing 5% CO_2 atmosphere at 37 °C.

In vitro CCK-8 Assay

The in vitro cytotoxicity of NRA@DH Gel against GL261 cells was evaluated using CCK-8 assay. In detail, GL261 cells were seeded on 96-well dishes at a density of 1×10^5 cells per well prior to the experiments (5% CO_2, 37 °C). When the density of cells reached 70~80%, the NRA@DH Gel or DH Gel with different concentrations were added, and continually incubated together for 24 h. Subsequently, CCK-8 reagents were added into each well and incubated for 1 h at 37 °C. Finally, the cell viability was evaluated by measuring the absorbance of each well at 450 nm using a microplate reader (Bio Tek, Synergy H4, USA).

In vitro Plate Clone Formation Assay

An in vitro plate clone formation assay was carried out here to determine the clonogenicity and regeneration ability of GL261 cells in the treatment of NRA@DH Gel under a radiation action. In detail, the GL261 cells were seeded and cultured into 6-well dishes for 24 h (10^6 cells $well^{-1}$) and then incubated with added NRA@DH Gel for 24 hours at different radiation doses (0, 2, 4, 6, and 8 Gy). After radiation, the cells were continually incubated for 10~14 days (5% CO_2, 37 °C) and then were stained with crystal violet, which was subsequently observed under a microscope.

In vitro Intracellular Imaging

The in vitro targeting capability of NRA@DH Gel for GL261 cells was evaluated by a confocal laser scanning microscopy (CLSM; Leica, DMi8, Germany). Herein the GL261 cells were seeded on chamber slides and placed in the 12-well plates, culturing for 24 hours (10^6 cells $well^{-1}$). The NRA@DH Gel was then added to each well and continually incubated for 24 hours at 37°C (ultimate concentration: 0.7 μg of As mL^{-1}). After the incubation of NRA@DH Gel, the chamber slides were fixed in 4% paraformaldehyde for 30 min and washed in phosphate buffered saline (PBS) three times. Finally, the fixed cells were stained with 50 μL 4′,6-diamidino-2-phenylindole (DAPI; 0.02%, blue-stained reagent) in the dark for 30 min and then observed the red fluorescence signals using CLSM.

Determination of Intracellular GSH/GSSH Levels in vitro

The intracellular GSH and GSSG contents were determined using a quantitative GSH/GSSG detection kit method. In detail, the GL261 cells were first seeded in a 6-cm dish and cultured overnight (10^6 cells $well^{-1}$). The cells were then incubated with PBS, NR@DH Gel, and NRA@DH Gel for 24 h (ultimate concentration: 1.0 μg of As mL^{-1}). The levels of GSH and GSSG were measured with above-mentioned detection kit per the manufacturer's instructions using a UV–vis spectrophotometer (Shimadzu, UV-2501PC, Japan) at 412 nm.

Determination of Intracellular ROS Levels in vitro

The intracellular ROS contents were determined using a quantitative ROS assay kit method. In detail, the GL261 cells were first seeded in a 96-well dish and cultured overnight (10^5 cells $well^{-1}$). The cells were then incubated with Rousp, PBS, Gel, NR@DH Gel, and NRA@DH Gel for 24 h (ultimate concentration: 1.0 μg of As mL^{-1}). The levels of ROS

were measured with above-mentioned detection kit per the manufacturer's instructions using a fluorescence microplate reader (BioTek, Synergy H4, USA) with excitation of a 488 nm filter and emission of a 525 nm filter.

Determination of Intracellular γH2AX Levels in vitro

The intracellular γH2AX contents were determined using by a γH2AX ELISA kit method. In detail, the GL261 cells were first seeded and cultured in a 6-well plate (37°C, 5% CO_2, 10^5 cells $well^{-1}$). The cells were treated according to the experimental conditions described, respectively, incubated with PBS, DH Gel, NR@DH Gel, and NRA@DH Gel, and treated with selective RT for 24 h (ultimate concentration: 1.0 μg of As mL^{-1}). The levels of γH2AX were measured with above-mentioned detection kit per the manufacturer's instructions using a microplate reader (Bio Tek, Synergy H4, USA) with the absorbance of each well at 450 nm.

In vitro Cell Apoptosis Assay

The NR@DH Gel or NRA@DH Gel-induced cell apoptosis under the influence of radiation was evaluated by imaging flow cytometry (IFC; Amnis, Flow sight, USA) via Annexin V-FITC/PI fluorescent detection kit. In detail, the GL261 cells were first seeded and cultured in a 6-well plate (37°C, 5% CO_2, 10^5 cells $well^{-1}$). The cells were treated according to the experimental conditions described, respectively, incubated with PBS, DH Gel, NR@DH Gel, and NRA@DH Gel, and treated with selective RT for 24 h (ultimate concentration: 1.0 μg of As mL^{-1}). The RT here was performed at a dose of 2 Gy (6MV, 500 cGy/min) using a X-ray linear accelerator at room temperature. By centrifugal selection (1000 rpm), the collected cells were subsequently washed three times with PBS and re-suspended in a 500 μL of binding buffer, and then labeled with 5 μL of an Annexin V-FITC/PI probe, with continuous coincubation for 10 min in the dark. The intracellular fluorescence intensity was detected using IFC and analyzed using IDEAS software V6.2.

In vitro Mitochondrial Membrane Potential Assay

Detection of the mitochondrial membrane potential (Ψ_m) was performed using a JC-1 assay kit and evaluated using IFC (Amnis, Flow sight, USA). In detail, the GL261 cells were first seeded and cultured in a 6-well plate (37°C, 5% CO_2, 10^5 cells $well^{-1}$). Then, the cells were, respectively, incubated with PBS, DH Gel, NR@DH Gel, and NRA@DH Gel, and treated with selective RT for 24 h (ultimate concentration: 1.0 μg of As mL^{-1}). By centrifugal selection (1000 rpm), the collected cells were washed three times with PBS and re-suspended in a 500 μL JC-1 working fluid and incubated for 15 min at 37 °C in the dark. The intracellular fluorescence intensity was detected using IFC and analysed using IDEAS software V6.2.

In vitro Transwell Migration Assay

The in vitro cell metastatic activity was evaluated by transwell migration assay using a matrigel membrane. In detail, the GL261 cells (3×10^4) were suspended in serum-free medium and seeded in the upper chamber, and then a DMEM medium with 10% FBS is added to the lower chamber. In different treatments, the cells were, respectively, incubated with PBS, DH Gel, NR@DH Gel, and NRA@DH Gel, and treated with selective RT for 48 h (ultimate concentration: 1.0 μg of As mL^{-1}). The bottom ventricle cells were finally fixed by 4% paraformaldehyde and stained with 0.1% crystal violet. The migrated cells were photographed and counted under a microscope.

Animal Protocol

The 6~8 weeks old C57BL/6 female mice were purchased from Beijing HFK Bioscience Co., Ltd., and fed in a specific-pathogen-free-level laboratory. For implantation, mice were anesthetized using 3% isoflurane in oxygen gas, and then the mice were placed in a stereotaxic apparatus, in situ injected of 5×10^5 GL261 cells. The coordinates were set as follows: 1 mm right lateral, 1 mm behind the intersection of the coronal and sagittal cranial sutures, 3.5 mm depth. All of the animal care and experimental procedures were performed in accordance with the Animal Management Rules and Guidelines of the Ministry of Health of the People's Republic of China and approved by the Animal Ethics Committee of Xuzhou Medical University and Jiangsu Normal University.

The GL261 tumor-bearing mice were divided randomly into seven groups: (1) saline as the control, (2) intratumor injection of empty Gel carrier, (3) intratumor injection of NR@DH Gel, (4) intratumor injection of NRA@DH Gel, (5) only RT administration alone, (6) intratumor injection of NR@DH Gel with RT action, and (6) intratumor injection of NRA@DH Gel with RT action. The mice were designed with intratumorally administered NRA@DH Gel (single dose of 0.85 mg of As kg^{-1} body weight) experimental group under radioactive ray exposure within two stages (with 7 days as a stage, a total of 14 days) of synergistic therapy combining RT with chemotherapy. The RT here was performed at a dose of 5 Gy (6MV, 500 cGy/min) using an X-ray linear accelerator.

In vivo Fluorescence Imaging

Real-time in vivo drug distribution in tumor tissue was carried out under an IVIS fluorescence imaging system (Caliper Life Sciences, USA) with excitation of 610 nm filter and emission of 840 nm filter. The in vivo fluorescence signal of the tumor area in mice was detected at different times during 0~6 day. Meanwhile, the CI values between the tumor tissue and adjacent normal brain tissue were calculated using the following formula: $CI = I_T/I_M$, where I_T was the average fluorescence signal of the tumor area and I_M was the signal of adjacent normal brain tissue calculated by using regions of interest (ROI) functions. To further observe the distribution of drug inside mice organs, normal organs such as heart, liver, kidneys, lungs, spleen, and tumor tissue were, respectively, stripped from the body for further ex vivo fluorescence detection.

Histological Examination

On the 16th day, the GL261 tumor-bearing mice in different groups were sacrificed, and major organs or tissue were stripped, fixed in 4% paraformaldehyde and subsequently embedded in paraffin at a thickness of 3~5 mm. In histological analysis, the tissue sections were then deparaffinized in xylene and finally sealed using neutral gum within hematoxylin and eosin (H&E) staining for optical microscope observation.

In immunohistochemical (IHC) staining, tumor paraffin slices were first dewaxed and rehydrated prior to antigen retrieval. Next, the slices were put into 3% H_2O_2 for 10 minutes to block endogenous peroxidase activity, and then blocked with 5% BSA for 1 h. After washing with PBS 3 times, the slices were incubated with primary antibodies (CD31, Ki-67, and HIF-1α) overnight at 4 °C, and subsequently incubated with HRP labeled goat anti-rabbit secondary antibodies (1:200) for 20 minutes. After adding the diaminobenzidine (DAB) chromogenic solution, the sections were incubated with a hematoxylin dye solution for 5 min and finally sealed with neutral gum for optical microscope observation.

In Masson trichrome staining, the tumor paraffin slices were dewaxed and rehydrated, then counterstained with hematoxylin for 5 min. After washing with distilled water 3 times, the slices were finally stained by Masson trichrome staining reagent according to the manufacturer's instructions for optical microscope observation.

Hematologic Examination

On the 16th day, the whole blood was collected from GL261 tumor-bearing mice and used for liver or kidney function and routine blood examination. All hematologic tests were provided by the Department of Laboratory Medicine of Xuzhou Central Hospital.

In vivo Western Blotting Assay

Invasion and migration-related proteins (Gpr56 and Flotillin-2) in tumor tissue were detected using a Western blotting (WB) assay. Specifically, here the tumor tissues were lysed on ice with RIPA buffer for 30 min, and centrifuged to obtain the supernatant proteins (12,000 rpm, 10 min). Then, BCA assay kit was used to quantitatively calculate the concentration of extracted proteins. Equal amounts of protein were separated by 10% SDS-PAGE and immediately transferred to PVDF membrane. Subsequently, the membrane was blocked with 5% BSA for 1 h followed by incubation with specific primary antibodies (anti-Gpr56, anti-Flotillin-2, and anti-β-actin) overnight at 4 °C. After washing with PBST for 3 times, the membranes were incubated with HRP-linked anti-rabbit IgG or anti-mouse IgG secondary antibodies (1:5000, Cell Signaling Technology, Inc., Beverly, MA, USA) for 1 hour at room temperature. Using an ECL chemiluminescent

kit (Pierce Biotechnology, Inc., Rockford, IL, USA) to detect the blots by an automatic chemiluminescence imaging analysis system (Amersham Imager 600, General Electric Company, MA, USA). Quantitative analysis of protein expression was analyzed using ImageJ software (Version 1.52v, National Institutes of Health, Bethesda, MD, USA).

In vivo Anti-Tumor Efficacy Evaluation

The in vivo anti-tumor efficacy was evaluated by tumor volume, mice body weight, and mice survival rate analysis. Tumor volumes were calculated from the H&E staining images of brain sections of orthotopic glioma-bearing mice and bioluminescence imaging in vivo after 16-day treatment in all groups. The mice body weight was measured every other day during 16 days' observation period. At the end of drug administration, the mice survival period and survival rate were also evaluated in different groups.

Behavioral Evaluation

Pressure on peripheral nervous system from advanced brain tumor may cause disorders of movement and balance ability in mice. Based on this, the behavioral evaluation of mice is a critical indicator for tumor therapeutic effect. The spontaneous locomotor activities of the mice were evaluated by open field test and rotarod test. Specifically, the mice in different groups were placed in the center of individual square box (45 cm × 45 cm) and allowed to freely explore the chamber for the duration of the 5 min test session, recorded by a real-time automatic camera system. In addition, the steps of the rotarod test were as follows: setting the starting speed of the rotarod to 5 rpm, the final speed to 40 rpm, the acceleration time to 5 min, and the running time to 5 min, to observe the movement state and time of the mice on the rod, repeated for each group for 3 times.

Results and Discussion

Synthesis and Characterization of NRA@DH Gel

Herein, we describe a novel method for synthesizing high-performance NRA QDs. Specifically, pure RP was first dispersed in functionalized NPC and PEG_{200} solution at high temperature (250 °C) via a coordination chemical reaction to form NR QDs with a carboxy terminus (NR-COOH QDs) by a nucleation and growth process. The use of NPC as an amino acid coating ligand was able to strongly coordinate with NR QDs. Then, NR-COOH QDs were further coupled with 6-AN molecules at their carboxyl terminus by the activation of EDC and NHS to produce NRA QDs as shown in Figure 1A.

Moreover, pH-sensitive DEX gel, a type of smart hydrogel, can be used as a carrier for sustained, controlled, and targeted drug release in situ. In the present study, DEX gel with multiple hydroxyl groups was firstly oxidized by $NaIO_4$ to form ODEX gel with an aldehyde terminus. After the addition of functionalized NPN molecules, pH-sensitive amide bonds were then introduced by a Schiff base reaction at the aldehyde groups of ODEX gel to form DEX gel with amino terminals (DEX-NH_2 gel). Next, DEX-NH_2 gel was coupled with activated HA molecules to form DEX-NH_2 gel with active targeting ability. Finally, the above-mentioned NRA QDs were encapsulated in DEX-HA gel by physical embedding to fabricate NRA@DH Gel. A detailed procedure for the synthesis of NRA@DH Gel is shown in Figure 1A.

The aim of the present study was to develop a multifunctional NRA@DH Gel capable of increasing intracellular ROS levels to increase tumor sensitivity to the combination of RT and NRA@DH Gel-mediated chemotherapy in vivo. The following characteristics of NRA@DH Gel were evaluated in the present study (Figure 1B): (1) active targeting following intratumoral administration in GL261 glioma tumor-bearing mice to enhance penetration and accumulation in tumor tissue and cells; (2) intracellular release of NRA QDs from pH-sensitive NRA@DH Gel in tumor acidic microenvironments; (3) the use of NRA@DH Gel as a competitive inhibitor of PPP metabolism; and (4) the synergistic effect of the combination of NRA@DH Gel-mediated RT and chemotherapy as a comprehensive tumor therapy. Note that the inhibitory effect of NRA@DH Gel on PPP metabolism improves the efficacy of RT by substantially reducing NADPH production, blocking the conversion of intracellular GSSG to GSH and stimulating continuous production of ROS to improve the efficacy of RT.

Synthesized NRA QDs encapsulated in gel had a brownish yellow appearance with good water solubility. TEM images demonstrated that NRA QDs are present as individual, well-defined spheres with an average size of 2–2.5 nm

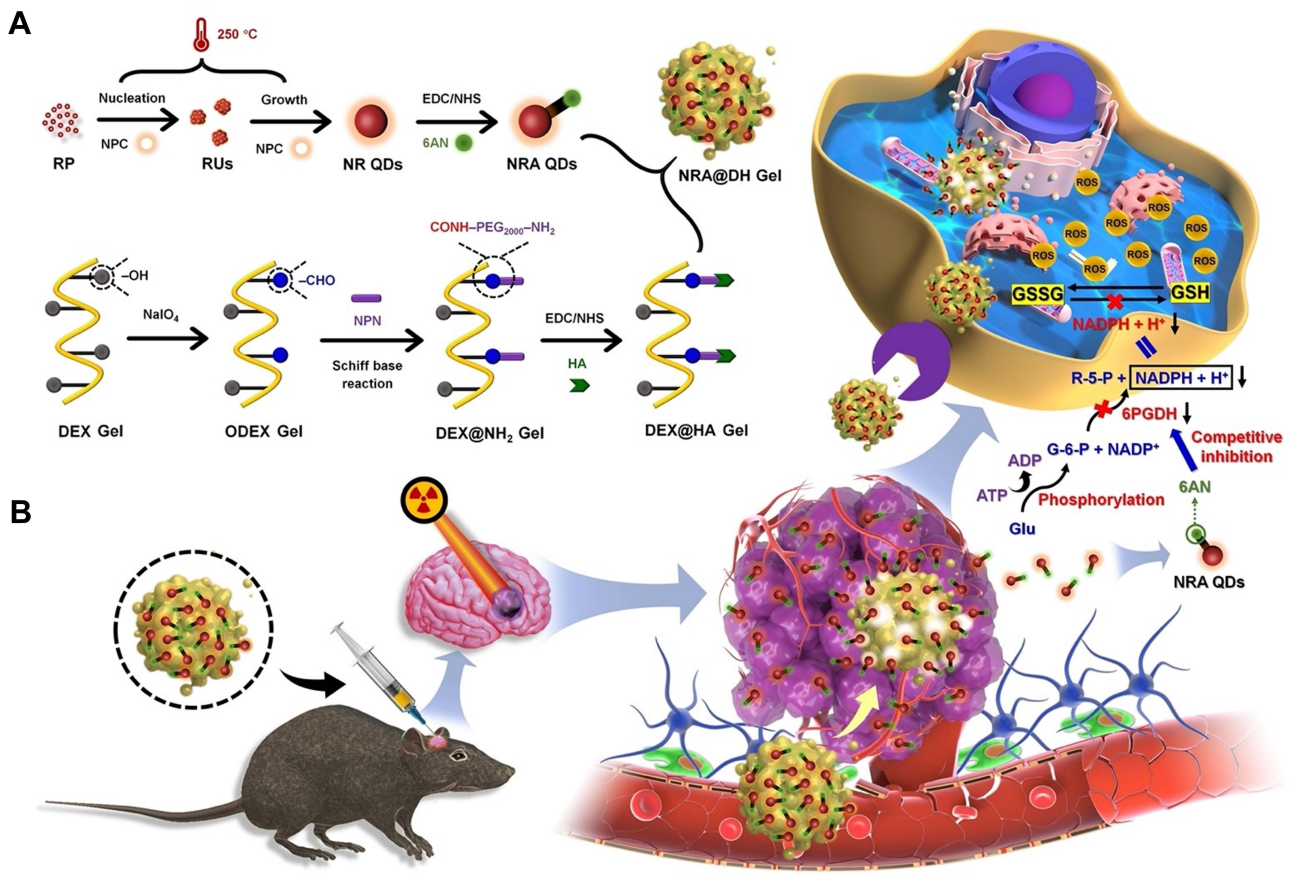

Figure 1 (**A**) Schematic illustration showing the synthesis of NRA QDs, DEX-HA gel, and multifunctional NRA@DH Gel. (**B**) Schematic representation of the in vivo mechanisms underlying synergistic therapy with NRA@DH Gel including accumulation in tumor tissues, deep penetration, and sustained ROS generation.

(Figure 2A). Further SEM examinations revealed that NRA@DH Gel has a clear three-dimensional (3D) network structure (Figure 2B). The inherent pore structure and connectivity improve the release of NRA QDs and match the structure of natural extracellular matrix (ECM) in vivo. Additional elemental distribution mappings confirmed the coexistence of As, S, and C elements in NRA@DH Gel with a uniform distribution (Figure 2B). Further, FTIR characteristic specific vibrations of NRA@DH Gel were present at 3450, 2875, 1650, and 1480 cm^{-1} which correspond to ν(O−H), ν(N−H), ν(CHO), ν(C=O), and ν(CONH) (Schiff's base bonds) stretching modes, respectively (Figure 2C). In addition, the observation of a peak at approximately 513 cm^{-1}, which corresponds to the stretching vibration of the S–S group, supports the presence of NR QDs in the NRA@DH Gel. In order to characterize our material more precisely, Raman spectroscopy was here used to characterize the characteristic structure of the NR QDs. Raman spectroscopy is able to express the characteristic peaks in the low-frequency region more precisely. The Raman characteristic peaks of NRA@DH Gel in low-frequency regions (150~400 cm^{-1}) consisted of three specific vibrations, As–As stretching at 185 cm^{-1}, As–S stretching at 270~300 cm^{-1}, and As–S–As bending at 221 cm^{-1} and 160 cm^{-1}, which verified the nature of realgar (Figure S1).

The optical properties of NRA@DH Gel were next evaluated. The UV−vis absorption of NRA@DH Gel exhibited strong broadband characteristic absorption within the range of 400–700 nm, which provides a basis for multiband excitation (Figure 2D). The fluorescent emission of NRA@DH Gel was characterized by optimal excitation at 610 nm with the largest emission peak observed at 840 nm (near-infrared region, Figure 2D). To further evaluate the photostability of the NRA@DH Gel, we evaluated fluorescence performance over placement time (1–30 days), with no obvious fluorescence loss observed over the study period indicating that NRA@DH Gel possesses high photostability (Figure 2E). The excellent optical properties of NRA@DH Gel are expected to provide a foundation for applications in cancer diagnosis and treatment.

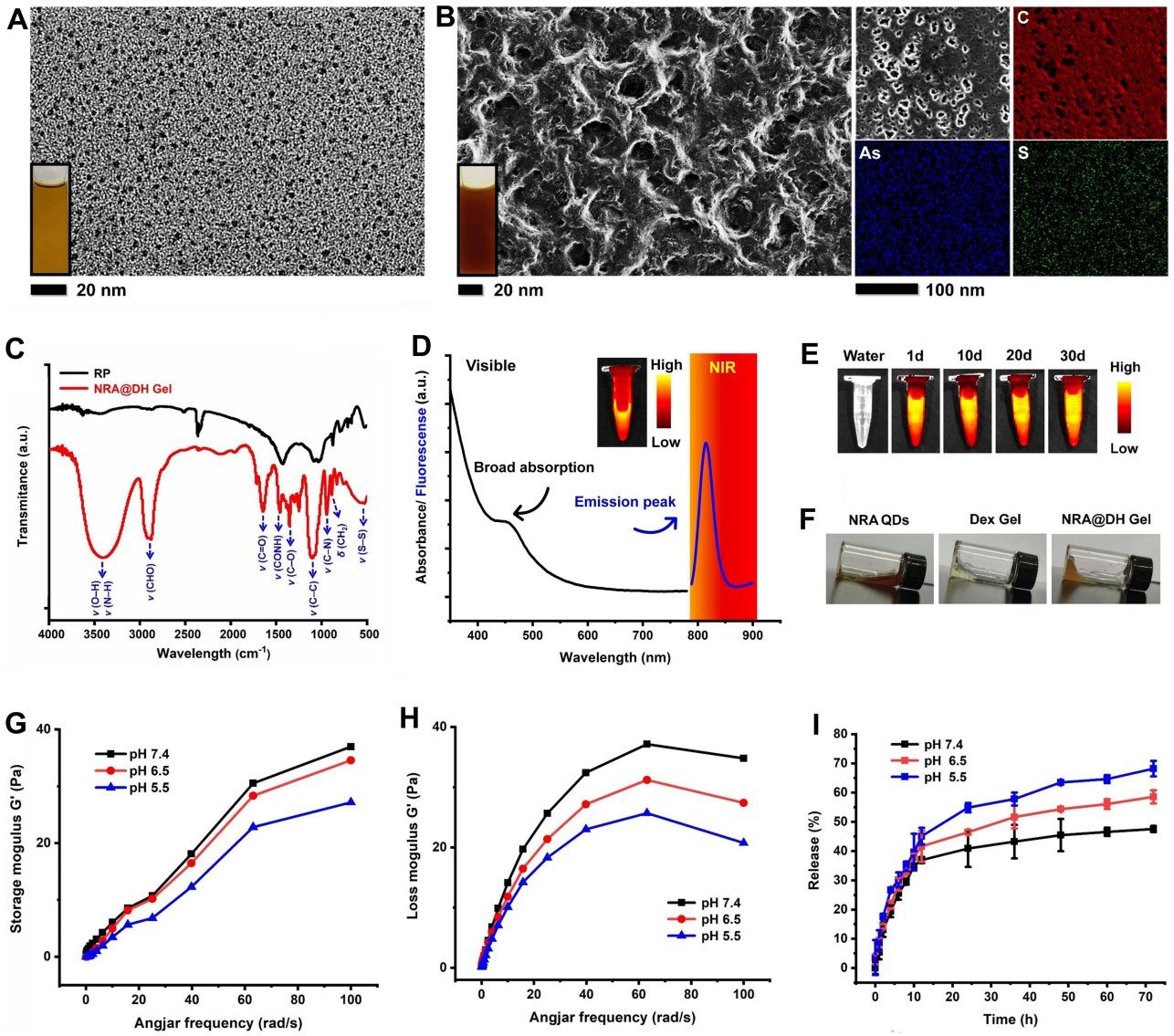

Figure 2 (**A**) TEM images of NRA QDs. (**B**) SEM image and corresponding elemental mapping images of NRA@DH Gel. (**C**) FT-IR spectra of pure RP and NRA@DH Gel. (**D**) UV−vis absorption and fluorescence spectra of NRA@DH Gel. (E_x = 610 nm; E_m = 840 nm). Inset shows fluorescent image. (**E**) Fluorescence stability of NRA@DH Gel after one month. (**F**) Photographs of NRA QDs, DEX gel, and NRA@DH Gel. (**G** and **H**) Rheological properties of NRA@DH Gel at varying pH levels. (**I**) pH-controlled encapsulated NRA QDS release curves for NRA@DH Gel at pH 7.4, 6.5, and 5.5 over 72 h.

In addition, the gelation behaviors of NRA@DH Gel were evaluated by rheological analyses. Compared with NRA QDs, NRA@DH Gel had greater viscosity, which increased the utility of NRA@DH Gel as a carrier for sustained, controlled, and targeted drug release (Figure 2F). We investigated the rheological properties of NRA@DH Gel using oscillatory rheology experiments with monitoring of variations in the storage modulus (G') and loss modulus (G") with angular frequency at room temperature (Figure 2G and H). Considering the use of intracranial in situ drug delivery in the present study, a soft hydrogel may decrease intracranial pressure thereby facilitating practical applications.[44,45] The G' and G" values of NRA@DH Gel were approximately the same throughout the experiment (0–100 s) at varying pH conditions, indicating that NRA@DH Gel is stable with good mechanical and gelation state properties.

In vitro Release of NRA QDs from NRA@DH Gel

Regulating the release of NRA QDs encapsulated within NRA@DH Gel is important for enhanced anti-tumor activity. Since tumor microenvironments are typically acidic, particularly inside lysosomes and endosomes within tumor cells, we

quantitatively evaluated in vitro drug release efficiency of pH-responsive NR-loaded gels in neutral and acidic conditions. NRA@DH Gel was incubated in phosphate buffer adjusted to pH 7.4, 6.5, and 5.5 at 37°C. NRA release curves at varying temperatures are shown in Figure 2I. pH-controlled NRA QDs release is mediated by the breaking of Schiff base bonds (containing C-N double bond of the imine or azomethine group) between amino groups (present in NPN) and aldehyde groups (present in oxidized DEX). Our results indicate that the structural stability of NRA@DH Gel is dependent on time and acidity, with the NRA QDs release rate from NRA@DH Gel comparatively lower at pH 7.4 (47.6%) but increased significantly at pH 6.5 (58.6%) and 5.5 (65.2%). Under acidic conditions, acid-sensitive Schiff base bonds in DEX macromolecules were broken, and encapsulated NRA QDs were released from the disintegrating NRA@DH Gel network structures.

In vitro Cytotoxicity

To validate the cytotoxicity of the NRA@DH Gel in vitro, we used CCK-8 assay kits to perform cytotoxicity assay in GL261 cells. As illustrated in Figure 3A, there was a trend toward decreasing cell viability with increasing concentrations of NRA@DH Gel. We calculated the IC_{50} value of NRA@DH Gel in GL261 cells as 0.7 As μg mL^{-1}. We also evaluated the toxicity of empty Dex-HA (DH) gel in GL261 cells (Figure 3B). DH Gel demonstrated negligible non-cytotoxicity with a cell viability greater than 80% when the concentrations of DH are lower than 12.5 mg mL^{-1}. The in vitro CCK8 results indicate that NRA@DH Gel has toxic effects on GL261 cells, with the inhibitory effect predominantly mediated by NRA QDs in concentration-dependent manner.

Mechanisms Underlying the Effect of NRA@DH Gel on Radiotherapy Sensitization

6-AN has been posited as an inhibitor of the oxidative pentose phosphate pathway by competitively inhibiting glucose-6-phosphate dehydrogenase and decreasing the production of NADPH, the primary cofactor involved in reducing glutathione (GSSG to GSH conversion) and reducing scavenging of ROS by GSH. To assess this proposed mechanism, we measured GSH and GSSG levels in GL261 cells following treatment with NRA@DH Gel. As shown in Figure 3C, higher concentrations of GSSG and lower concentration of GSH were observed in cells treated with NRA@DH Gel compared with the control group, indicating NRA@DH Gel is an inhibitor of the oxidative PPP and reduces the activity of GSH, thereby acting as a sensitizing agent for RT.

Interestingly, we found that NR@DH Gel without 6-AN also induced substantial changes in GSH concentration, indicating that NR QDs may have GSH-scavenging properties. To verify this finding, we measured GSH concentrations in GL261 cells in response to treatment with different doses of NR QDs. As shown in Figure 3D, GSH concentrations decreased as NR QD concentration increased. This finding indicates that the effect of NR QDs on GSH levels may be attributable to arsenic in realgar forming conjugates with GSH, thereby reducing the amount of dissociative GSH in cells and disturbing the equilibrium between oxidation and reduction.[46,47] In addition, we verified the total concentration of ROS in cells in response to different treatments. As shown in Figure 3E, a significant increase in ROS level was detected after treatment GL261 cells with NRA@DH Gel compared with the control group and other treated groups. The increased generation of intracellular reactive ROS may lead to the accumulation of reactive ROS leading to oxidative damage and RT sensitization. Finally, the in vitro radio-sensitization efficacy of NRA@DH Gel was measured by colony formation (Figure 3F and G). As predicted, NRA@DH Gel with RT successfully suppressed the proliferation of cancer cells with a sensitization enhancement ratio (SER) value of 1.654, demonstrating the substantial potential of NRA@DH Gel as a radiosensitizer. Overall, NRA@DH Gel decreases GSH levels and increases ROS production, thereby indicating the efficacy of NRA@DH Gel in enhancing the efficacy of RT.

In vitro Targeting Effect

As the NRA@DH Gel was coupled with the targeting ligand HA, NRA@DH Gel specifically bound CD44 (the HA receptor) on the surface of tumor cells, thereby increasing intracellular enrichment and anti-tumor activity.[48,49] The cellular uptake of NRA@DH Gel is a critical determinant of targeting ability. Given the excellent fluorescence performance, we used CLSM to track the red fluorescence of NRA@DH Gel to evaluate cell-specific targeting (Figure 3H). CLSM images of cells demonstrated a large portion of overlapping red (NRA@DH Gel) and blue

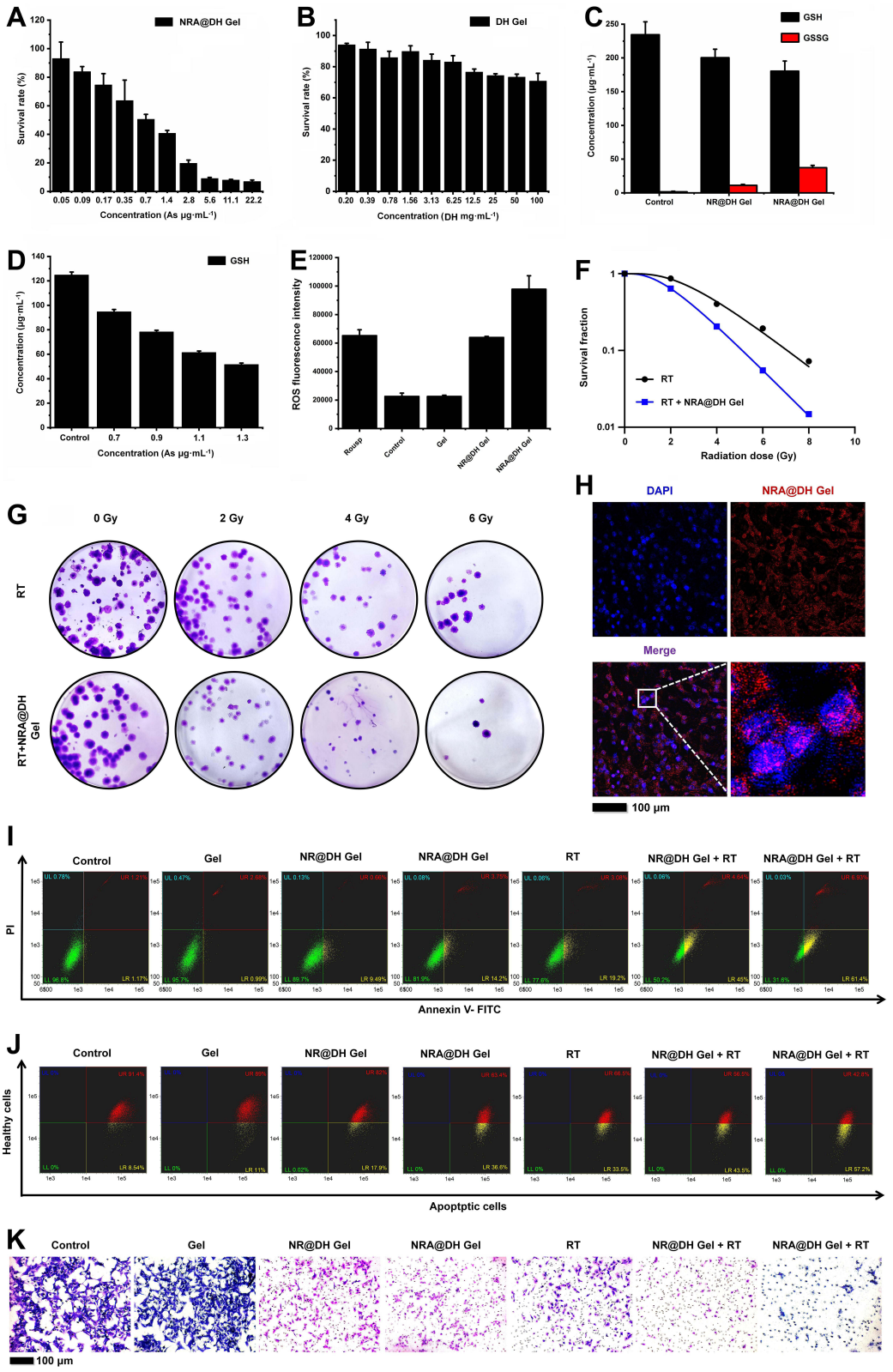

Figure 3 (**A**) Concentration-dependent cell viability of GL261 cells after treatment with NRA@DH Gel and (**B**) empty DH Gel. (**C**) Concentration of GSH/GSSG after different treatments in GL261 cells. (**D**) The concentration of GSH after treatment with different concentrations of NRA QDs in GL261 cells. (**E**) Fluorescence intensity of ROS after different treatments in GL261 cells. (**F**) Digital images of colony formation after treatment with PBS and NRA@DH Gel under 0, 2, 4, and 6 Gy radiation. (**G**) Colony formation curves of GL261 cells treated with PBS and NRA@DH Gel under 2, 4, 6 and 8 Gy radiation. (**H**) Specific nuclear targeting effect of NRA@DH Gel on GL261 cells observed by CLSM. Cell nuclei stained with DAPI are shown in blue and fluorescent NRA@DH Gel is shown in red. (**I**) Apoptosis and necrosis in response to different treatments as measured by Annexin V-FITC/PI double staining detected by FCM. (**J**) Changes in $\Delta\Psi m$ using JC-1 dye as detected by FCM following different treatments. (**K**) In vitro metastatic activity of GL261 cells determined by transwell migration assay in response to different treatments.

(DAPI, nuclear dye) fluorescence after incubation with NRA@DH Gel for 24 h, indicating that NRA@DH Gel was able to enter cells through targeted endocytosis. To measure the specificity of NRA@DH Gel for HA receptors on a cytomembrane, we performed a competition assay by pre-treating GL261 cells with free HA as a competitive inhibitor and then incubating cells with NRA@DH Gel at the same concentration. The observation of a weak intracellular red fluorescence signal demonstrated decreased cellular uptake of NRA@DH Gel indicating that cellular internalization of NRA@DH Gel is medicated by HA receptor-mediated endocytosis, thereby increasing enrichment at tumor sites (Figure S2).

In vitro Anti-Tumor Efficacy

Apoptosis and changes in mitochondrial membrane potential are the two main mechanisms underlying the anti-tumor effects of NRA@DH Gel in vitro. First, we used an Annexin V-FITC/PI double staining flow cytometry (FCM) approach to compare NRA@DH Gel-induced apoptosis in GL261 cells following exposure to selective RT compared to the control group (Figure 3I). The apoptotic rate in GL261 cell was calculated as the total percentage of early and late apoptosis cells (indicated by LR and UR in a quadrantal diagram). As shown in Figure 3I, apoptosis rates were significantly higher in the NR@DH Gel (10.15%) and NRA@DH Gel group (17.95%) than in the control group (2.38%) and gel group (3.67%), indicating that NR QDs and NRA QDs have significant in vitro anti-tumor activity. Compared with NR@DH Gel group, the apoptosis rates of NRA@DH Gel group were higher, this may be related to the addition of 6-AN, which increase the concentration of GSSG and ROS and damage cells. However, cell apoptosis rates reached 49.64% and 68.33% in cells treated with NR@DH Gel or NRA@DH Gel in combination with RT, while cells treated with RT only had cell apoptosis rates of 22.28%. These apoptosis rates indicate that chemotherapy with NR@DH Gel or NRA@DH Gel in combination with RT is more effective in increasing apoptosis in GL261 cells.

Numerous studies have reported that almost all mitochondrial structures and functions are affected during the early stages of apoptosis, including decreases in mitochondrial membrane potential. Accordingly, we used JC-1 dye as an indicator of changes in mitochondrial membrane potential ($\Delta_{\Psi m}$) by fluorescence emission displacement as the proportion of J-aggregates (intact state, red fluorescence) converted to J-monomers (impaired state, green fluorescence).[50] As shown in Figure 3J, no significant changes in $\Delta_{\Psi m}$ were observed in the control (10.70) and gel groups (8.09) with the ratio of J-aggregate and J-monomers, respectively. Treatment with NR@DH Gel and NRA@DH Gel led to significant decreases in the ratio to 4.58 and 1.73, respectively, NRA@DH Gel Group decreased more than NR@DH Gel group, indicating that drug hydrogels are able to induce apoptosis by damaging DNA structure and depolymerizing J-aggregates into J-monomers, and NRA@DH Gel led to more decrease than NR@DH Gel. After combining NR@DH Gel or NRA@DH Gel treatment with RT, the radio decreased to 1.30 and 0.75, respectively, indicating further break down of J-aggregates into J-monomers. These results demonstrate that treatment with NR@DH Gel or NRA@DH Gel combined with RT has a synergistic effect on decreasing the mitochondrial membrane potential of tumor cells.

To further explore the DNA damage, we measured γH2AX protein levels in GL261 cells following treatment using ELISA (Figure S3). We can see that compared with the control group and the gel group, the γH2AX protein content in the NR@DH Gel and NRA@DH Gel groups is significantly increased, which proves that drugs can cause DNA damage, and the γH2AX protein content is higher when NR@DH Gel and NRA@DH Gel are combined with radiotherapy compared with RT only. It proved that treatment with NR@DH Gel or NRA@DH Gel combined with RT has a synergistic effect on increasing DNA damage.

In addition, in vitro cell metastatic activity was evaluated by transwell migration assay using Matrigel membranes (Figure 3K). Greater decreases in invasiveness and migration were observed in cells (purple staining) treated with NRA@DH Gel and RT compared with other groups. The results of these in vitro anti-tumor assays demonstrate the substantial potential of NRA@DH Gel as an optimized therapeutic agent for synergistic cancer therapy in vivo.

In vivo Tissue Accumulation and Metabolism of NRA@DH Gel

To evaluate tissue accumulation and metabolism of NRA@DH Gel in vivo, we established an in-situ mouse model of glioblastoma using GL261 cells. Mice received intratumoral injection of NRA QDs or NRA@DH Gel (0.5 mg of As kg^{-1} body weight). Real-time in vivo fluorescence imaging was used to track the accumulation and retention of NRA

QDs or NRA@DH Gel in tumor tissue over a 6-day period, as shown in Figure 4A. A strong fluorescence signal was observed in tumor tissue on the first day after intratumoral injection of NRA@DH Gel, with the fluorescence signal slowly decreasing between days 2 and 6 before falling to a nadir on day 6 after administration. In contrast, no discernible fluorescence signal was observed at tumor sites in the NRA QDs group at day 3 after administration due to poor accumulation, poor retention, and relatively short duration in the systemic circulation. Compared with smaller-sized NRA QDs, larger-sized NRA@DH Gel had a more pronounced aggregation effect at tumor sites. To quantitatively evaluate the circulation, accumulation, and metabolism of NRA QDs and NRA@DH Gel in a time-dependent manner, we calculated the corresponding contrast index (CI) values between tumor tissue and adjacent normal brain tissue (Figure 4B). CI values on days 2 and 3 after the administration of NRA@DH Gel were 5.88 and 3.82, respectively, higher values than

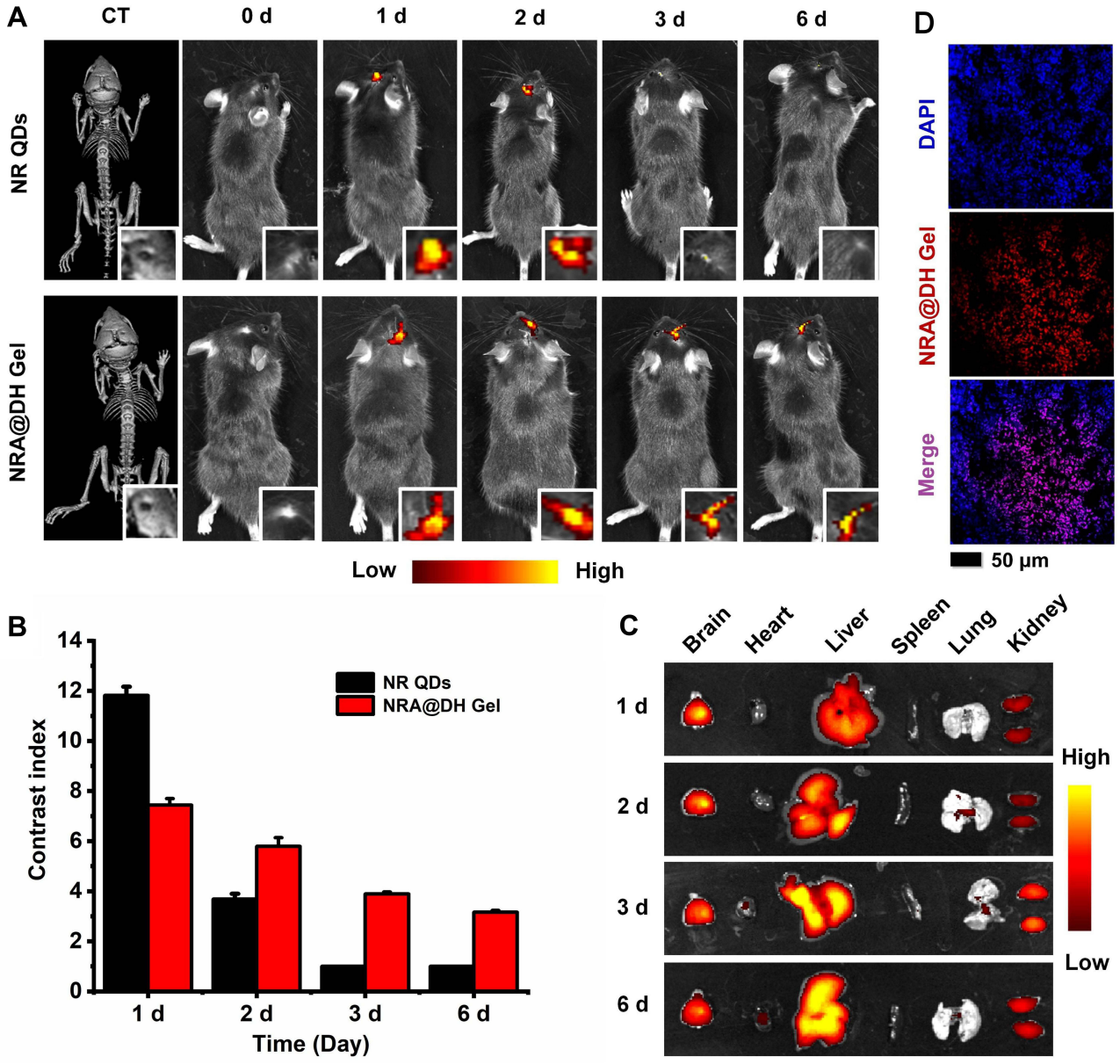

Figure 4 (**A**) Real-time in vivo fluorescence images (Ex = 610 nm; Em = 840 nm) of GL261 tumor- bearing mice after intratumoral injection of NRA QDs and NRA@DH Gel over a 6-day period (administered dose, 0.5 mg As kg^{-1} body weight). (**B**) Corresponding fluorescence signal-based CI values at tumor sites and adjacent normal brain tissue at different times post-administration (0–6 days). (**C**) Ex vivo fluorescence imaging of heart, liver, spleen, lung, kidneys, and tumor tissues collected after the injection of NRA@DH Gel at different times post-administration (1, 2, 3, and 6 days). (**D**) CLSM images of tumor cryosections after treatment with fluorescent NRA@DH Gel. Cell nuclei stained with DAPI are shown in blue and NRA@DH Gel is shown in red.

following the administration NRA QDs (3.72 and 1.04, respectively). NRA@DH Gel maintained a CI value of 3.21 over the next 3 days, demonstrating superior retention in tumor tissues. Our results indicate that the use of hydrogel as a drug carrier allows slow release of NRA QDs in vivo, prolonging the duration of action.

To better understand the metabolism of NRA QDs, we dissected and immediately collected major organs (heart, liver, spleen, lungs, and kidneys) and tumors for further ex vivo fluorescence imaging following treatment with NRA@DH Gel. Fluorescence signals were predominantly observed in tumor tissue, liver, and kidneys over the study period, indicating that NRA QDs were gradually cleared by liver- and kidney-mediated metabolic processes (Figure 4C). In addition, we further investigated the intracellular localization of NRA QDs released from NRA@DH Gel in tumor tissues at 48 h post-administration using CLSM imaging of cryosections (Figure 4D). Substantial NRA QDs aggregates with red fluorescence were observed throughout intracellular structures including the cytoplasm and nuclear membrane, indicating NRA QDs were efficiently taken up via HA receptor-mediated endocytosis or were internalized into tumor connective tissue. These findings are consistent with the results of in vivo and ex vivo fluorescence imaging.

In vivo Anti-Tumor Efficiency

The demonstration of substantial accumulation of NRA@DH Gel in tumor tissues indicates the potential of NRA QDs as an anti-tumor therapy. After demonstrating the accumulation and retention of NRA@DH Gel in tumor tissues by in vivo fluorescence imaging over a period of 6 days, we next evaluated an optimized in vivo therapeutic strategy in a murine model of intracranial glioblastoma. At 7 days after intracranial GL261 inoculation, mice developed significant dysmotility symptoms, indicating successful establishment of the intracranial glioma model. Mice then received intratumoral administration of NRA@DH Gel (single dose of 0.85 mg As kg^{-1} body weight) combined with RT in two stages (RT at days 7 and 14; Figure 5A). Mice were randomly divided into seven groups as follows: (1) intratumoral injection of saline as a control, (2) intratumoral injection of empty gel carrier, (3) intratumoral injection of NR@DH Gel, (4) intratumoral injection of NRA@DH Gel, (5) RT only, (6) intratumoral injection of NR@DH Gel with RT, and (7) intratumoral injection of NRA@DH Gel with RT.

After 16 days of treatment, mice were sacrificed and tumor tissues were sectioned and stained with H&E (Figure 5B). H&E staining revealed greater tissue injury and necrosis including decreased cell density, nuclear shrinkage, and fragmentation in tumor tissues from the NRA@DH Gel and RT treatment group compared to other groups. Additionally, significant tumor cell injury was observed in the NR@DH Gel with RT treatment group, NR@DH Gel treatment group, NRA@DH Gel treatment group, and RT only treatment group. Normal tumor cell morphology was observed in the empty gel treatment group and control group. The histogram of the necrosis rate in different groups was added into Figure S4. In addition, the anti-tumor efficacy of treatments was further investigated in tumor ECM composed of dense collagen (blue-stained) and muscle fibers (red-stained) by Masson's trichrome staining (Figure 5B). Collagen is a major component of ECM, where a higher stromal content of dense collagen is associated with poor survival outcomes, which compresses and distorts tumor blood vessels and acts as a physical barrier to drug delivery. NRA@DH Gel combined with RT had the greatest suppressive effect on the growth of collagen fibroblasts and lowest muscle fiber density compared to other treatments, thereby enhancing NRA@DH Gel penetration of tumor tissues. The inhibition of cancer-associated ECM activity disturbs the tumor microenvironment, indicating the synergistic effect of NRA@DH Gel and RT in the treatment of tumors.

The in vivo anti-tumor efficacy of NRA@DH Gel was also evaluated by IHC staining of tumor tissues. To our knowledge, the presence of hypoxic regions in solid tumors may decrease NRA@DH Gel-mediated sensitivity to radiotherapy, chemotherapy, and combinatorial treatment in GL261 cells. Accordingly, increasing the targeting of NRA@DH Gel to tumor tissues may improve tumor oxygenation, thereby enhancing the efficacy of RT. Anti-hypoxia-inducible factor 1 alpha (HIF-1α) antibody staining is routinely used for the evaluation of hypoxic states in tumor tissues. HIF-1α is an oxygen regulated subunit of HIF-1. HIF-1α levels are determined by tumor oxygen levels, which have been shown to be associated with resistance to radiotherapy and chemotherapy.[51] The results of IHC staining demonstrated that HIF-1α protein expression (marked in brown) was significantly lower following treatment with NRA@DH Gel (Figure 5C). This finding indicates that the hypoxic state of tumors may be alleviated by NRA@DH Gel treatment by improving tumor oxygenation and enhancing the effect of NRA@DH Gel on radio-sensitization. In

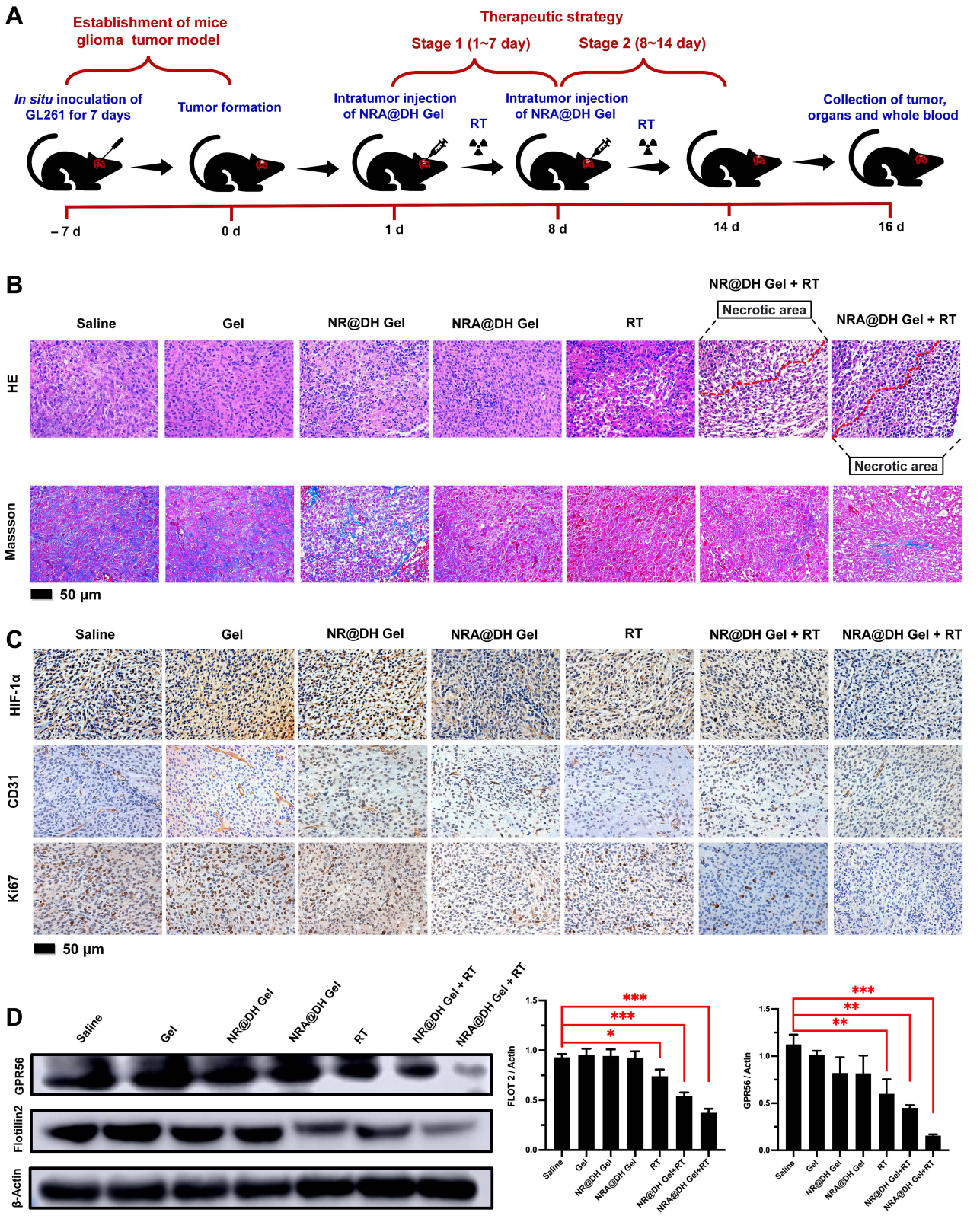

Figure 5 (**A**) Experimental schematic of NRA@DH Gel- mediated synergistic therapy in two stages (7 days per stage for a total of 14 days, single dose of 0.85 mg As kg^{-1} body weight). GL261 tumor-bearing mice were randomly divided into seven groups. (**B**) Images of H&E and Masson staining of tumor tissues after 16 days of treatment. (**C**) IHC staining for HIF-1α, CD31 and Ki-67 in tumor tissue sections after 16 days of treatment. (**D**) Western blotting of Flot 2 and GPR 56 in tumor tissues from GL261 tumor -bearing mice (*p < 0.05, **p< 0.01, ***p < 0.001).

https://doi.org/10.2147/IJN.S394377 DovePress

addition, IHC staining for CD31 and Ki-67 was performed to evaluate tumor angiogenesis, cell proliferation, and migration,[52,53] as shown in Figure 5C. As expected, CD31 and Ki-67 expression levels in tumors treated with NRA@DH Gel and RT were significantly lower compared to other treatments, indicating NRA@DH Gel inhibits cell proliferation and migration and has a suppressive effect on tumor microvasculature. These findings highlight the potential of NRA@DH Gel as a synergistic therapy in vivo. The semi-quantitatively of immunohistochemical was added in Figure S5.

To determine the mechanisms underlying the anti-tumor effects of NRA@DH Gel, we performed WB of Gpr56 and Flotillin-2, proteins involved in tumor migration and invasion (Figure 5D and Figure S8). Gpr56 protein, which is secreted by a range of tumor types, plays a crucial role in cancer metastasis.[54] Flotillin-2 protein has been shown to increase tumor invasion.[55] As predicted, Gpr56 and Flotillin-2 protein levels in tumors treated with NRA@DH Gel combined with RT were significantly lower than in other groups, demonstrating a synergistic effect of treatment with NRA@DH Gel and RT on inhibiting tumor angiogenesis and suppressing tumor migration and invasion. The results of WB are consistent with the aforementioned IHC staining results.

To evaluate tumor growth over time, we performed H&E staining of brain tissue sections from orthotopic glioma-bearing mice and bioluminescence imaging in vivo after 16 days of treatment in all groups (Figure 6A-C). H&E staining and luminescence intensity in tumors indicated that the NRA@DH Gel and RT synergistic treatment group had the smallest tumor size compared to other treatment groups. Quantitative luminescence analysis of tumor area ratio (TAR) at day 16 and day 1 demonstrated greater suppression of tumor growth in the NRA@DH Gel combined with RT treatment group, with an inhibition TAR value of 0.30 compared to the NR@DH Gel combined with RT treatment group (0.58), NRA@DH Gel treatment group (0.95), NR@DH Gel treatment group (3.82), RT only treatment group (1.09), gel only treatment group (11.25), and saline treatment group (14.38). These results indicate that NRA@DH Gel combined with RT treatment group had the greatest inhibitory effect on tumor growth.

Safety Evaluations

Mice were sacrificed on day 16 and evaluated for toxic side effects on major organs including the heart, liver, spleen, lung, and kidneys by H&E staining. No significant morphological changes were observed in major organs in any treatment group, indicating minimal systemic toxicity, or damage to normal tissues during treatment with NR@DH Gel, NRA@DH Gel, or RT (Figure 6D). Blood was collected for routine serological examinations and assessment of liver and kidney function (Figure 6E). Routine serological parameters [white blood cells (WBC), red blood cells (RBC), blood platelet (PLT), hemoglobin (HGB), hematocrit (HCT), erythrocyte mean corpuscular volume (MCV), mean corpuscular hemoglobin (MCH)] and markers of liver and kidney function [aspartate aminotransferase (AST), alkaline phosphatase (ALP), albumin (ALB), blood urea nitrogen (BUN), uric acid (UA), and creatinine (CREA)] remained at normal levels in the NR@DH Gel and NRA@DH Gel treatment groups, indicating good hematological, liver, and kidney safety profiles. In addition, mice body weights were recorded over the 16 days of treatment. Blood routine tests and liver and kidney function tests of mice treated with NRA QDs alone found that both blood routine and liver function were within the normal range. However, the parameter of kidney function of the mice showed low values compared to the other treatment groups, demonstrating the lower metabolic toxicity of the NRA QDs alone (Figure S6). No variations in body weight over the study period were observed in NR@DH Gel or NRA@DH Gel treatment groups, indicating that mice tolerated repeated administration of NR@DH Gel and NRA@DH Gel (Figure 6F). We previously conducted a trial and found that the change in NRA QDs treatment groups in weight was not significantly abnormal compared to the saline group (Figure S7).

Behavioral Evaluations

Pressure on peripheral nerves due to advanced brain tumors may cause disorders of movement and poor balance in mice. Accordingly, we performed behavioral evaluations of mice as a critical indicator of therapeutic effect.[56] On day 16, we, respectively, selected open field experiments and rotating rod experiments to evaluate changes in mobility and balance in mice after treatment with NR@DH Gel or NRA@DH Gel (Figure 7A-C). The open field experiment allows the assessment of a range of behaviors in animals when entering an open environment and is used to evaluate locomotor ability and mental state in mice. As shown in Figure 7A and B, the normal mice group moved 3100–3300 cm, while mice

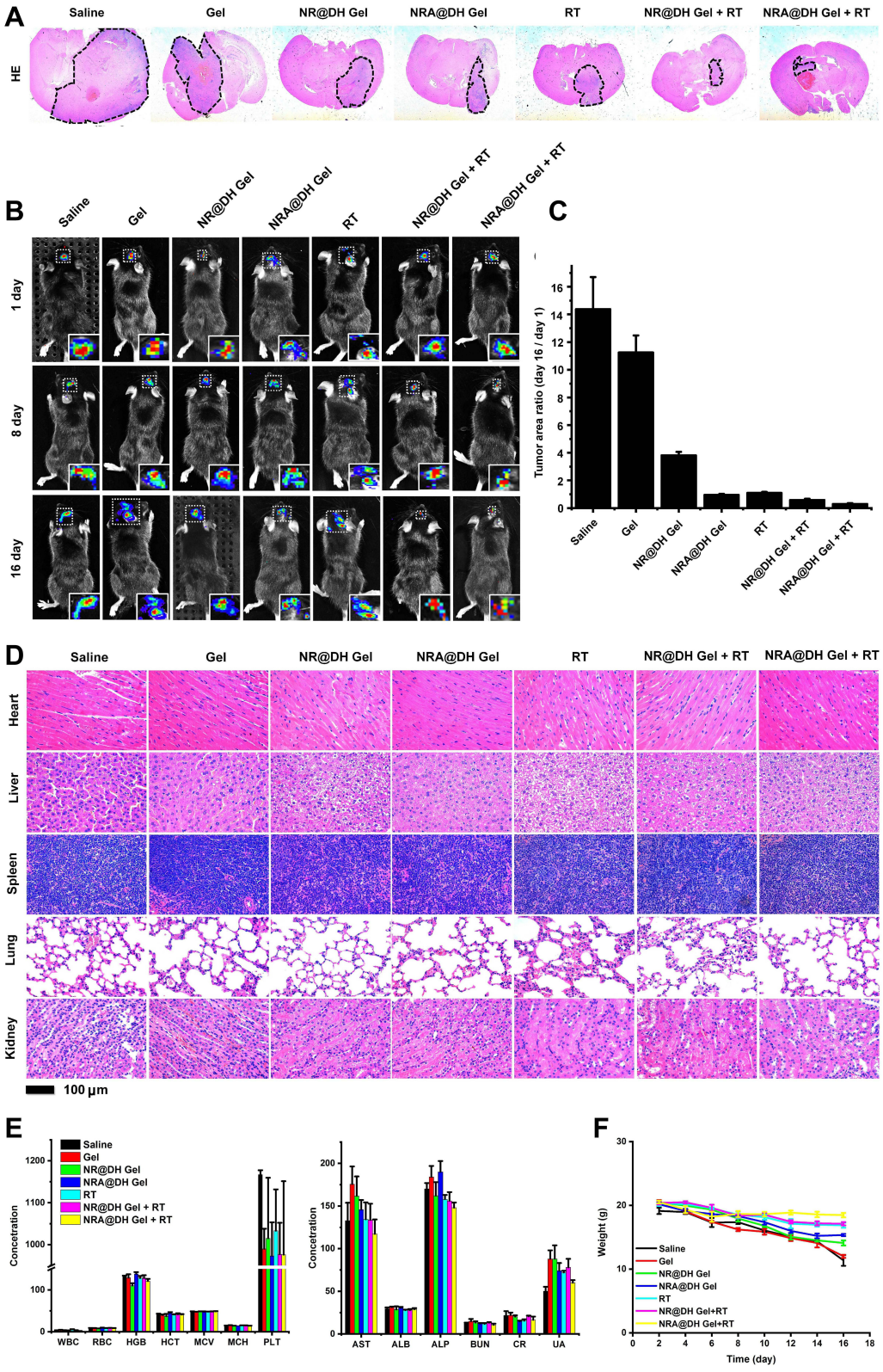

Figure 6 (**A**) H&E staining of murine brain tissue following different treatments over a period of 16 days. (**B**) In vivo bioluminescence in glioma-bearing mice following different treatments at 1, 8, and 16 days. (**C**) Quantitative bioluminescence analysis of tumor area ratio (TAR) at day 16 and day 1. (**D**) Images of H&E staining of normal organ tissues from mice after 16 days of treatment. (**E**) Routine serological parameters (WBC, RBC, PLT, HGB, HCT, MCV, and MCH) and liver and kidney function parameters (AST, ALP, ALT, BUN, and CREA) in blood collected from mice. (**F**) Body weight changes in indicated groups over the 16-day observation period.

https://doi.org/10.2147/IJN.S394377 DovePress

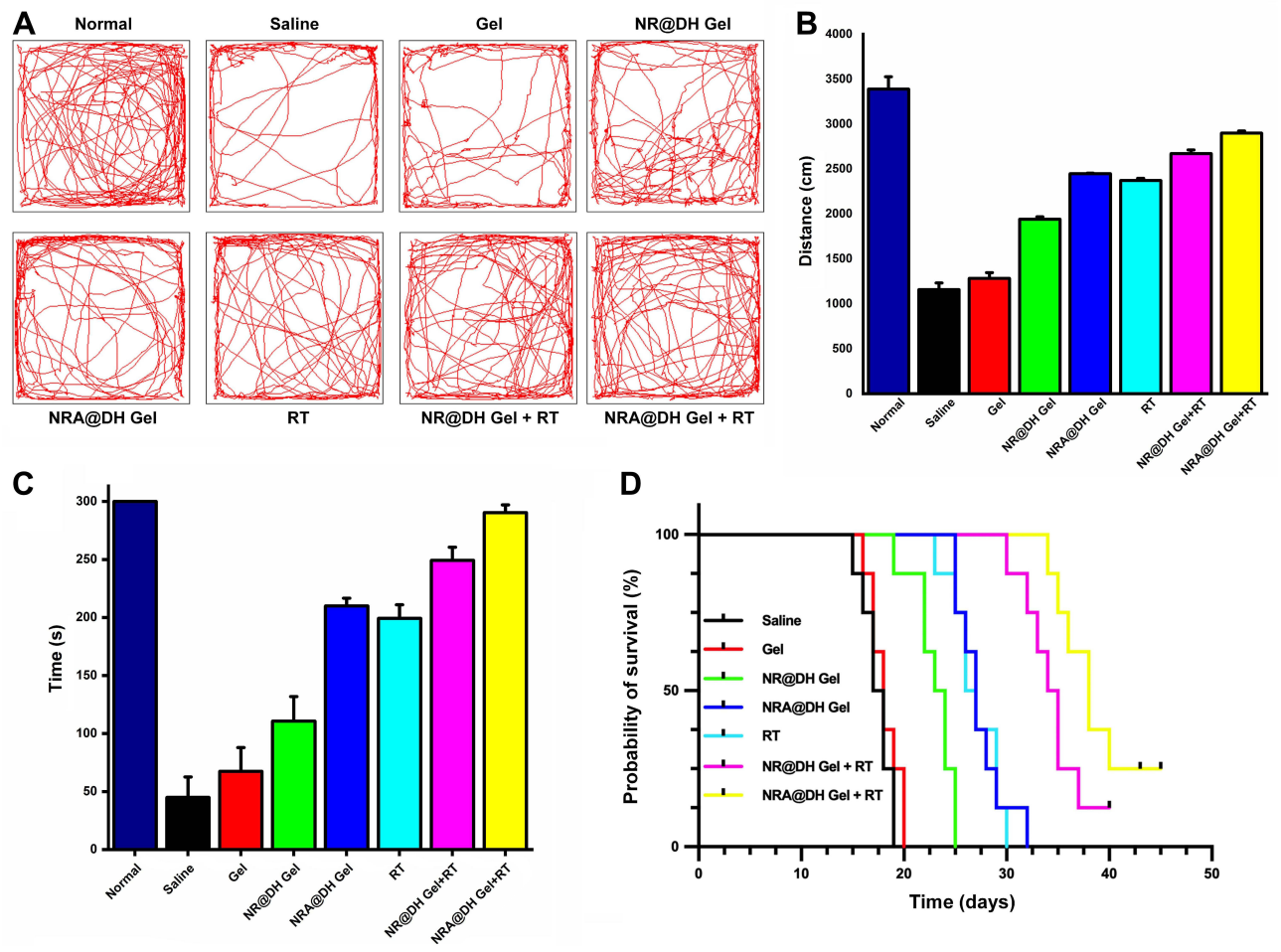

Figure 7 (**A**) Trajectory maps and (**B**) numerical statistics of open field tests in different groups. (**C**) Numerical statistics from the rotarod test in different groups. (**D**) Survival curves of mice in different groups (n = 8 per group).

in the saline group moved the least miles, basically around approximately 1000–1200 cm, mice. Mice paused more often in the field and moved essentially only as they moved around the field. The motor mileage of the tumor distance traveled by tumor-bearing mice in the gel administration gel treatment group was 1200–1300 cm, indicating that the empty gel did not have a gel that had no significant alleviating effect on glioma-induced dyskinesia. In contrast, the NR@-DH Gel administration gel treatment group, the NRA@-DH Gel administration gel treatment group, and the RT only treatment group of mice showed some improved demonstrated greater locomotor performance by reaching travelling 1900–2000 cm, 2400–2500 cm, and 2300–2400 cm, respectively, after treatment. The NRA@DH Gel administration in combination with RT synergistically treated group of tumor-bearing mice could reach a motor course. Tumor-bearing mice treated with NRA@DH Gel combined with RT traveled more than 2800 cm, which was not significantly different from normal mice, indicating that the NRA@DH Gel-mediated synergistical treatment could significantly inhibit glioma and improve limb movement in mice.

The rotating rods experiments evaluate the motor coordination of mice by measuring sense of balance, which is an important tool for evaluating the effects of drugs on the central nervous system. As seen in Figure 7C, mice in the NRA@DH Gel and RT treatment group had a longer stick time (292 s) compared to the saline and other treatment groups, indicating combinatorial treatment with NRA@DH Gel and RT had the greatest effect on locomotion and balance. NRA@DH Gel combined with RT significantly prolonged survival in mice by an average of 40 days compared to normal saline and other treatment groups.

Through NRA@DH Gel and RT combination therapy, the survival of mice was prolonged to an average of 38 days, with statistically significant differences versus normal saline and other treatment groups (Figure 7D).

Conclusion

In summary, the present study demonstrates the successful fabrication of a functional herbal medicine NRA@DH Gel with active targeting properties and pH-responsiveness. As a traditional drug in a modified administration form, NRA@DH Gel demonstrated potent anti-tumor activity. As a fluorescent probe, NRA@DH Gel emitted fluorescence up to the near-infrared region and had excellent bioimaging properties, indicating the utility of NRA@DH Gel in the evaluation and treatment of tumor-bearing mice. NRA@DH Gel allows sustained drug release in the acidic environment of the tumor microenvironment of glioma in mice. The enclosed NRA QDs were shown to inhibit PPP metabolism and reduce the production of NADPH, thereby inhibiting the conversion of GSSG to GSH, reducing GSH concentrations in tumor cells, promoting the accumulation of ROS, and improving the tumor hypoxic environment. Each of these effects contributes to the significant RT sensitizing properties of NRA@DH Gel. Through the synergistic effect of chemotherapy and RT, NRA@DH Gel effectively inhibited the proliferation and migration of tumor cells, suppressed tumor growth, improved motor coordination, and prolonged survival in tumor-bearing mice. We believe NRA@DH Gel represents a highly effective chemotherapeutic agent with fluorescence properties, which can be combined with RT to achieve the goal of "new applications of old drugs" for the traditional Chinese medicine realgar and allow applications in future clinical treatments.

Acknowledgments

This research was supported by the National Natural Science Foundation of China (81672973, 81701821), Major Fundamental Research Program of Natural Science Foundation of Jiangsu Higher Education Institution of China (16KJB310003), Medical leaders Foundation of Xuzhou City (XWRCHT20210023), Science and Technology program projects of Xuzhou City (KC21188).

Disclosure

The authors report no conflicts of interest in this work.

References

1. van Solinge TS, Nieland L, Chiocca EA, Broekman MLD. Advances in local therapy for glioblastoma — taking the fight to the tumour. *Nat Rev Neurol*. 2022;18(4):221–236. doi:10.1038/s41582-022-00621-0
2. Madani F, Esnaashari SS, Webster TJ, Khosravani M, Adabi M. Polymeric nanoparticles for drug delivery in glioblastoma: state of the art and future perspectives. *J Control Release*. 2022;349:649–661. doi:10.1016/j.jconrel.2022.07.023
3. Madhavan K, Balakrishnan I, Lakshmanachetty S, et al. Venetoclax Cooperates with Ionizing Radiation to Attenuate Diffuse Midline Glioma Tumor Growth. *Clin Cancer Res*. 2022;28(11):2409–2424. doi:10.1158/1078-0432.Ccr-21-4002
4. van den Bent MJ, Tesileanu CMS, Wick W, et al. Adjuvant and concurrent temozolomide for 1p/19q non-co-deleted anaplastic glioma (CATNON; EORTC study 26053-22054): second interim analysis of a randomised, open-label, Phase 3 study. *Lancet Oncology*. 2021;22(6):813–823. doi:10.1016/s1470-2045(21)00090-5
5. Erel-Akbaba G, Carvalho LA, Tian T, et al. Radiation-Induced Targeted Nanoparticle-Based Gene Delivery for Brain Tumor Therapy. *Acs Nano*. 2019;13(4):4028–4040. doi:10.1021/acsnano.8b08177
6. Zhang J, Chen Y, Fang J. Targeting thioredoxin reductase by micheliolide contributes to radiosensitizing and inducing apoptosis of HeLa cells. *Free Radic Biol Med*. 2022;186:99–109. doi:10.1016/j.freeradbiomed.2022.05.007
7. Cheng K, Sano M, Jenkins CH, et al. Synergistically Enhancing the Therapeutic Effect of Radiation Therapy with Radiation Activatable and Reactive Oxygen Species-Releasing Nanostructures. *ACS Nano*. 2018;12(5):4946–4958. doi:10.1021/acsnano.8b02038
8. Rey S, Schito L, Koritzinsky M, Wouters BG. Molecular targeting of hypoxia in radiotherapy. *Adv Drug Deliv Rev*. 2017;109:45–62. doi:10.1016/j.addr.2016.10.002
9. Kaushik N, Kaushik NK, Choi EH, Kim JH. Blockade of Cellular Energy Metabolism through 6-Aminonicotinamide Reduces Proliferation of Non-Small Lung Cancer Cells by Inducing Endoplasmic Reticulum Stress. *Biology*. 2021;10(11). doi:10.3390/biology10111088
10. Sharma PK, Bhardwaj R, Dwarakanath BS, Varshney R. Metabolic oxidative stress induced by a combination of 2-DG and 6-AN enhances radiation damage selectively in malignant cells via non-coordinated expression of antioxidant enzymes. *Cancer Lett*. 2010;295(2):154–166. doi:10.1016/j.canlet.2010.02.021
11. Varshney R, Adhikari JS, Dwarakanath BS. Contribution of oxidative stress to radiosensitization by a combination of 2-DG and 6-AN in human cancer cell line. *Indian J Exp Biol*. 2003;41(12):1384–1391.

12. Koutcher JA, Alfieri AA, Matei C, Meyer KL, Street JC, Martin DS. Effect of 6-aminonicotinamide on the pentose phosphate pathway: 31P NMR and tumor growth delay studies. *Magnetic resonance in medicine*. *1996-Dec*. 1996;36(6):887–892. doi:10.1002/mrm.1910360611
13. Wen S, Ovais M, Li X, et al. Tailoring bismuth-based nanoparticles for enhanced radiosensitivity in cancer therapy. *Nanoscale*. 2022;14 (23):8245–8254. doi:10.1039/d2nr01500e
14. Zhou X, You M, Wang F, et al. Multifunctional Graphdiyne–Cerium Oxide Nanozymes Facilitate MicroRNA Delivery and Attenuate Tumor Hypoxia for Highly Efficient Radiotherapy of Esophageal Cancer. *Adv Mater*. 2021;33(24):e2100556. doi:10.1002/adma.202100556
15. Bhardwaj P, Goda JS, Pai V, et al. Ultrasound augments on-demand breast tumor radiosensitization and apoptosis through a tri-responsive combinatorial delivery theranostic platform. *Nanoscale*. 2021;13(40):17077–17092. doi:10.1039/d1nr04211d
16. Zhang X-D, Luo Z, Chen J, et al. Ultrasmall Au 10−12 (SG) 10−12 Nanomolecules for High Tumor Specificity and Cancer Radiotherapy. *Adv Mater*. 2014;26(26):4565–4568. doi:10.1002/adma.201400866
17. Zhao J, Wang Y, Huang X, et al. Liu Shen Wan inhibits influenza virus-induced secondary Staphylococcus aureus infection in vivo and in vitro. *J Ethnopharmacol*. 2021;277:114066. doi:10.1016/j.jep.2021.114066
18. Ma W, Yue J, Liang S, et al. Realgar increases defenses against infection by Enterococcus faecalis in Caenorhabditis elegans. *J Ethnopharmacol*. 2021;268:113559. doi:10.1016/j.jep.2020.113559
19. Xu W, Chen Z, Shen X, Pi C. Reno-Protective Effect of Realgar Nanoparticles on Lupus Nephritis of MRL/Lpr Mice through STAT1. *Iranian J Immunol Spr*. 2019;16(2):170–181. doi:10.22034/iji.2019.80260
20. Ma H, Kou J, Zhu D, Yan Y, Yu B. Liu-Shen-Wan, a traditional Chinese medicine, improves survival in sepsis induced by cecal ligation and puncture via reducing TNF-alpha levels, MDA content and enhancing macrophage phagocytosis. *Int Immunopharmacol*. 2006;6(8):1355–1362. doi:10.1016/j.intimp.2006.03.003
21. Dagher T, Maslah N, Edmond V, et al. JAK2(V617F) myeloproliferative neoplasm eradication by a novel interferon/arsenic therapy involves PML. *J Exp Med*. 2021;218:(2)e20201268. doi:10.1084/jem.20201268
22. Cui Z, Zhang Y, Xia K, et al. Nanodiamond autophagy inhibitor allosterically improves the arsenical-based therapy of solid tumors. *Nat Commun*. 2018;9(1):4347. doi:10.1038/s41467-018-06749-2
23. Kutny MA, Alonzo TA, Gerbing RB, et al. Arsenic Trioxide Consolidation Allows Anthracycline Dose Reduction for Pediatric Patients With Acute Promyelocytic Leukemia: report From the Children's Oncology Group Phase III Historically Controlled Trial AAML0631. *J Clin Oncol*. 2017;35 (26):3021–3029. doi:10.1200/JCO.2016.71.6183
24. Dilda PJ, Hogg PJ. Arsenical-based cancer drugs. *Cancer Treat Rev*. 2007;33(6):542–564. doi:10.1016/j.ctrv.2007.05.001
25. Wang T, Meng J, Wang C, et al. Inhibition of Murine Breast Cancer Metastases by Hydrophilic As4S4 Nanoparticles Is Associated With Decreased ROS and HIF-1alpha Downregulation. *Front Oncol*. 2019;9:333. doi:10.3389/fonc.2019.00333
26. Zhu HH, Wu DP, Jin J, et al. Oral tetra-arsenic tetra-sulfide formula versus intravenous arsenic trioxide as first-line treatment of acute promyelocytic leukemia: a multicenter randomized controlled trial. *J Clin Oncol*. 2013;31(33):4215–4221. doi:10.1200/JCO.2013.48.8312
27. Wang T, Zhang X, Jia M, et al. Hydrophilic Realgar Nanocrystals Prolong the Survival of Refractory Acute Myeloid Leukemia Mice Through Inducing Multi-Lineage Differentiation and Apoptosis. *Int J Nanomedicine*. 2022;17:2191–2202. doi:10.2147/IJN.S358469
28. Wang S, Liu X, Wang S, et al. Imatinib co-loaded targeted realgar nanocrystal for synergistic therapy of chronic myeloid leukemia. *J Control Release*. 2021;338:190–200. doi:10.1016/j.jconrel.2021.08.035
29. Cholujova D, Bujnakova Z, Dutkova E, et al. Realgar nanoparticles versus ATO arsenic compounds induce in vitro and in vivo activity against multiple myeloma. *Br J Haematol*. 2017;179(5):756–771. doi:10.1111/bjh.14974
30. Tian Y, Wang X, Xi R, et al. Enhanced antitumor activity of realgar mediated by milling it to nanosize. *Int J Nanomedicine*. 2014;9:745–757. doi:10.2147/IJN.S56391
31. Shi D, Pu S, Yin H, et al. Fluorescent Realgar Nanoclusters for Nuclear Targeting-Triggered Tumor Theranostics. *ACS Applied Nano Materials*. 2022;5(5):6485–6499. doi:10.1021/acsanm.2c00577
32. Wu JZ, Chen G, Shao YB, et al. Fluorescent Realgar Quantum Dots: new Life for an Old Drug. *Nano*. 2016;11. doi:10.1142/s1793292016500053
33. Wang H, Liu Z, Gou Y, et al. Apoptosis and necrosis induced by novel realgar quantum dots in human endometrial cancer cells via endoplasmic reticulum stress signaling pathway. *Int J Nanomedicine*. 2015;10:5505–5512. doi:10.2147/IJN.S83838
34. Wang J, Loh KP, Wang Z, et al. Fluorescent nanogel of arsenic sulfide nanoclusters. *Angew Chem Int Ed Engl*. 2009;48(34):6282–6285. doi:10.1002/anie.200900586
35. Wang JZ, Lin M, Zhang TY, et al. Arsenic(II) sulfide quantum dots prepared by a wet process from its bulk. *J Am Chem Soc*. 2008;130(35):11596. doi:10.1021/ja804436w
36. Zhang Y, Feng Z, Liu J, et al. Polarization of tumor-associated macrophages by TLR7/8 conjugated radiosensitive peptide hydrogel for overcoming tumor radioresistance. *Bioactive Materials*. 2022;16:359–371. doi:10.1016/j.bioactmat.2021.12.033
37. Luo FQ, Xu W, Zhang JY, et al. An Injectable Nanocomposite Hydrogel Improves Tumor Penetration and Cancer Treatment Efficacy. *Acta Biomater*. 2022;147:235–244. doi:10.1016/j.actbio.2022.05.042
38. Hivare P, Gangrade A, Swarup G, et al. Peptide functionalized DNA hydrogel enhances neuroblastoma cell growth and differentiation. *Nanoscale*. 2022;14(24):8611–8620. doi:10.1039/d1nr07187d
39. Wen Y, Liu Y, Zhang H, et al. A responsive porous hydrogel particle-based delivery system for oncotherapy. *Nanoscale*. 2019;11(6):2687–2693. doi:10.1039/c8nr09990a
40. Zhang W, Shi Y, Li H, et al. In situ injectable nano-complexed hydrogel based on chitosan/dextran for combining tumor therapy via hypoxia alleviation and TAMs polarity regulation. *Carbohydr Polym*. 2022:288119418. doi:10.1016/j.carbpol.2022.119418
41. Wu S, Yang Y, Wang S, et al. Dextran and peptide-based pH-sensitive hydrogel boosts healing process in multidrug-resistant bacteria-infected wounds. *Carbohydr Polym*. 2022;278:118994. doi:10.1016/j.carbpol.2021.118994
42. Zhang M, Chen G, Lei M, Lei J, Li D, Zheng H. A pH-sensitive oxidized-dextran based double drug-loaded hydrogel with high antibacterial properties. *Int J Biol Macromol*. 2021;182:385–393. doi:10.1016/j.ijbiomac.2021.03.169
43. Zhang X, Zhang T, Ma X, et al. The design and synthesis of dextran-doxorubicin prodrug-based pH-sensitive drug delivery system for improving chemotherapy efficacy. *Asian J Pharm Sci*. 2020;15(5):605–616. doi:10.1016/j.ajps.2019.10.001
44. Chatterjee S, Hui PC, Wat E, Kan CW, Leung PC, Wang W. Drug delivery system of dual-responsive PF127 hydrogel with polysaccharide-based nano-conjugate for textile-based transdermal therapy. *Carbohydr Polym*. 2020;236:116074. doi:10.1016/j.carbpol.2020.116074

45. Qu J, Zhao X, Ma PX, Guo B. pH-responsive self-healing injectable hydrogel based on N-carboxyethyl chitosan for hepatocellular carcinoma therapy. *Acta Biomater*. 2017;58:168–180. doi:10.1016/j.actbio.2017.06.001
46. Liu T, Sun L, Zhang Y, Wang Y, Zheng J. Imbalanced GSH/ROS and sequential cell death. *J Biochem Mol Toxicol*. 2022;36(1):e22942. doi:10.1002/jbt.22942
47. Zheng CY, Lam SK, Li YY, Ho JC. Arsenic trioxide-induced cytotoxicity in small cell lung cancer via altered redox homeostasis and mitochondrial integrity. *Int J Oncol*. 2015;46(3):1067–1078. doi:10.3892/ijo.2015.2826
48. Hou Y, Jin J, Duan H, et al. Targeted therapeutic effects of oral inulin-modified double-layered nanoparticles containing chemotherapeutics on orthotopic colon cancer. *Biomaterials*. 2022;283:121440. doi:10.1016/j.biomaterials.2022.121440
49. Yang Z, Luo H, Cao Z, et al. Dual-targeting hybrid nanoparticles for the delivery of SN38 to Her2 and CD44 overexpressed human gastric cancer. *Nanoscale*. 2016;8(22):11543–11558. doi:10.1039/c6nr01749e
50. Xue X, You S, Zhang Q, et al. Mitaplatin increases sensitivity of tumor cells to cisplatin by inducing mitochondrial dysfunction. *Mol Pharm*. 2012;9(3):634–644. doi:10.1021/mp200571k
51. Yong Y, Zhang C, Gu Z, et al. Polyoxometalate-Based Radiosensitization Platform for Treating Hypoxic Tumors by Attenuating Radioresistance and Enhancing Radiation Response. *ACS Nano*. 2017;11(7):7164–7176. doi:10.1021/acsnano.7b03037
52. Robillard L, Liao M, Minh N, Harding TC, Simmons AD, Dusek RL. The Multi-Kinase Inhibitor Lucitanib Enhances the Antitumor Activity of Coinhibitory and Costimulatory Immune Pathway Modulators in Syngeneic Models. *J Immunother*. 2022;45(8):335–348. doi:10.1097/cji.0000000000000427
53. Dowsett M, Nielsen TO, A'Hern R, et al. Assessment of Ki67 in breast cancer: recommendations from the International Ki67 in Breast Cancer working group. *J Natl Cancer Inst*. 2011;103(22):1656–1664. doi:10.1093/jnci/djr393
54. Yang L, Friedland S, Corson N, Xu L. GPR56 Inhibits Melanoma Growth by Internalizing and Degrading Its Ligand TG2. *Cancer Res*. 2014;74(4):1022–1031. doi:10.1158/0008-5472.Can-13-1268
55. Li X, Zhao S, Fu Y, et al. miR-34a-5p functions as a tumor suppressor in head and neck squamous cell cancer progression by targeting Flotillin-2. *Int J Biol Sci*. 2021;17(15):4327–4339. doi:10.7150/ijbs.64851
56. Bellinzona M, Roser F, Matthies C, Samii M, Saini M. Biopolymer-mediated suramin chemotherapy in the treatment of experimental brain tumours. *Acta Oncol*. 2004;43(3):259–263. doi:10.1080/02841860310023129